

Development of a ceramic gas-electron-multiplier neutron detector prototype with a large sensitive area

Lin Zhu(朱林), Jianrong Zhou(周健荣), Xiaojuan Zhou(周晓娟), Lixin Zeng(曾莉欣), Liang Xiao(肖亮), Hong Xu(许虹), Fei Jia(贾飞), Chaoyue Zhang(张超月), Yezhao Yang(杨烨钊), Dingfu Li(黎定福), Hao Xiong(熊皓), Yuguang Xie(谢宇广), Yubin Zhao(赵豫斌), Yadong Wei(魏亚东), Zhijia Sun(孙志嘉), and Yuanbo Chen(陈元柏)
Citatio: Chin. Phys. B, 2025, 34 (**9**): 090701. DOI: 10.1088/1674-1056/ade38a
http://cpb.iphy.ac.cn; http://iopscience.iop.org/cpb

What follows is a list of articles you may be interested in

Vector magnetometry in zero bias magnetic field using nitrogen-vacancy ensembles

Chunxing Li(李春兴), Fa-Zhan Shi(石发展), Jingwei Zhou(周经纬), and Peng-Fei Wang(王鹏飞)
Chin. Phys. B, 2024, 33 (**10**): 100701. DOI: 10.1088/1674-1056/ad73af

Performance optimization of scintillator neutron detectors for EMD in CSNS

Xiaojie Cai(蔡小杰), Qian Yu(于潜), Chang Huang(黄畅), Bin Tang(唐彬), Shihui Zhou(周诗慧), Xiaohu Wang(王小胡), Xiuping Yue(岳秀萍), and Zhijia Sun(孙志嘉)
Chin. Phys. B, 2023, 32 (**11**): 110701. DOI: 10.1088/1674-1056/acd8a2

A stopping layer concept to improve the spatial resolution of gas-electron-multiplier neutron detector

Jianjin Zhou(周建晋), Jianrong Zhou(周健荣), Xiaojuan Zhou(周晓娟), Lin Zhu(朱林), Jianqing Yang(杨建清), Guian Yang(杨桂安), Yi Zhang(张毅), Baowei Ding(丁宝卫), Bitao Hu(胡碧涛), Zhijia Sun(孙志嘉), Limin Duan(段利敏), and Yuanbo Chen(陈元柏)
Chin. Phys. B, 2022, 31 (**5**): 050702. DOI: 10.1088/1674-1056/ac398e

Design of a novel correlative reflection electron microscope for *in-situ* real-time chemical analysis

Tian-Long Li(李天龙), Zheng Wei(魏征), and Wei-Shi Wan(万唯实)
Chin. Phys. B, 2021, 30 (**12**): 120702. DOI: 10.1088/1674-1056/ac0522

Response of HD-V2 radiochromic film to argon ions

Lei Cheng(程蕾), Zhe Zhang(张喆), Guiyun Liang(梁贵云), and Yutong Li(李玉同)
Chin. Phys. B, 2021, 30 (**8**): 080702. DOI: 10.1088/1674-1056/ac077f

---

INSTRUMENTATION AND MEASUREMENT

Development of a ceramic gas-electron-multiplier neutron detector prototype with a large sensitive area

Lin Zhu(朱林)[1,2], Jianrong Zhou(周健荣)[1,2,3,†], Xiaojuan Zhou(周晓娟)[1,2,‡], Lixin Zeng(曾莉欣)[1,2], Liang Xiao(肖亮)[1,2], Hong Xu(许虹)[1,2], Fei Jia(贾飞)[1,2], Chaoyue Zhang(张超月)[1,2], Yezhao Yang(杨烨钊)[4], Dingfu Li(黎定福)[4], Hao Xiong(熊皓)[4], Yuguang Xie(谢宇广)[1,3], Yubin Zhao(赵豫斌)[1,2,3], Yadong Wei(魏亚东)[4], Zhijia Sun(孙志嘉)[1,2,3], and Yuanbo Chen(陈元柏)[1,2,3]

[1] *State Key Laboratory of Particle Detection and Electronics, Institute of High Energy Physics, Chinese Academy of Sciences, Beijing* 100049, *China*
[2] *Spallation Neutron Source Science Center, Dongguan* 523803, *China*
[3] *University of Chinese Academy of Sciences, Beijing* 100049, *China*
[4] *Institute of Science & Technology Innovation, Dongguan University of Technology (Institute of Science & Technology Innovation and Advanced Manufacturing), Dongguan* 523803, *China*

(Received 30 April 2025; revised manuscript received 4 June 2025; accepted manuscript online 11 June 2025)

The rapid growth of neutron flux has driven the development of ^{3}He-free neutron detectors to satisfy the requirements of the neutron scattering instruments under construction or planned at the China Spallation Neutron Source (CSNS). Position-sensitive neutron detectors with a high counting rate and large area play an important role in the instruments performing neutron measurements in or close to the direct beam. The ceramic gas-electron-multiplier (GEM) detector serves as a promising solution, and considerable work has been done using the small-area GEM neutron detectors. In this article, we designed and constructed a detector prototype utilizing ceramic GEM foils with an effective area of about 307 mm×307 mm. To evaluate and investigate their basic characteristics, the Monte Carlo (MC) tool FLUKA was employed and several neutron beam tests were conducted at CSNS. The simulated spatial resolution was basically in agreement with the measured value of 2.50±0.01 mm (FWHM). The wavelength spectra measurement was verified through comparisons with a commercial beam monitor. In addition, a detection efficiency of 4.7±0.1% was achieved for monoenergetic neutrons of 1.59 Å wavelength. This is consistent with the simulated result. The results indicate that the large-area ceramic GEM detector is a good candidate to implement neutron beam measurements. Its efficiency can be improved in a cascading manner to approach that reached by traditional ^{3}He detectors.

Keywords: neutron detector, counting rate, gas electron multiplier, spatial resolution, detection efficiency

PACS: 07.07.Df, 29.40.Gx, 28.20.Pr, 61.05.F–

DOI: 10.1088/1674-1056/ade38a **CSTR:** 32038.14.CPB.ade38a

1. Introduction

In recent decades, the rapid development of neutron scattering and imaging technologies has been promoted with the construction of pulsed spallation neutron facilities, such as the Spallation Neutron Source (SNS) in the US,[1] the ISIS Neutron and Muon Source (ISIS) in the UK,[2] the the Japan Proton Accelerator Research Complex (J-PARC) in Japan,[3] the China Spallation Neutron Source (CSNS) in China[4] and the European Spallation Source (ESS) in Europe.[5] These neutron sources offer pulsed time-dependent high flux neutrons, allowing for measurements of neutron energy or wavelength by the time-of-flight (TOF) method. CSNS is a large scientific facility that can provide a high-flux neutron beam produced by a high-energy proton pulse impacting a tungsten–tantalum (W–Ta) target. It has realized steady operation of 170 kW power with 25 Hz repetition frequency since autumn 2024. It will be upgraded to the designed power of 500 kW during the second phase of CSNS. At present, four neutron scattering instruments have been built and are open to users. They are the small angle scattering spectrometer (SANS),[6] the multi-purpose reflectometer (MR), [7] the general-purpose powder diffractometer (GPPD),[8] and the multi-physics instrument (MPI).[9] For these instruments, operated at the spallation neutron source delivering a high flux beam, a neutron detector with a large detection area plays a critical and essential role in instrument performance.

The detection of thermal neutrons is through an indirect process in which neutrons are first converted into charged particles by a nuclear reaction and then these released products are recorded. Conventional neutron detectors are proportional gaseous ones based on helium-3, due to their achievable high detection efficiency for thermal neutrons and excellent neutron/gamma discrimination. They mainly include counting tubes, linear position-sensitive detectors (LPSDs) and multi-wire proportional chambers (MWPCs). Unfortunately, these

†Corresponding author. E-mail: zhoujr@ihep.ac.cn
‡Corresponding author. E-mail: xjzhou@ihep.ac.cn

© 2025 Chinese Physical Society and IOP Publishing Ltd. All rights, including for text and data mining, AI training, and similar technologies, are reserved.

detectors have a low counting rate of a few tens of kHz due to saturation effects associated with the accumulation of space charge.[10] Meanwhile, the price of ^{3}He gas has risen sharply due to the ^{3}He crisis in 2008,[11] which has limited the large-scale application of ^{3}He-based detectors in newly built neutron scattering instruments. Therefore, it is urgent to find effective substitutes for ^{3}He gas and to develop new neutron detectors to meet the demands of the instruments under construction and/or upgradation at CSNS. As an ideal replacement for the ^{3}He, boron-10 (^{10}B) has a large absorption cross-section of about 4000 barns for 1.8 Å neutrons and high abundance in nature. A common method for detecting thermal neutrons is via ^{10}B, where a solid-state converter based on boron-containing material is appended to the gaseous detector. A neutron conversion layer containing ^{10}B is manufactured by heat-evaporation or magnetron sputtering techniques, which is cost-effective, physically and chemically stable, and environmentally friendly.

In measurements in or close to direct neutron beams, such as MR and SANS, the very small-angle neutron scattering instrument (VSANS) and the energy-resolved neutron imaging instrument (ENRI), the neutron detectors have to be irradiated in the high-flux environment and to work steadily. This operation condition necessitates a large detection area to ensure a wide coverage of the scattering angle, as well as a high counting rate capacity to achieve an extensive dynamic measurement range. It requires a two-dimensional (2D) position sensitive detector with a large effective area and an upper limit of counting rate of over 1 MHz. The gas electron multiplier (GEM), a micro-pattern gas detector, offers remarkable counting rate capacity ($\sim$ 10 MHz), good intrinsic resolution of space and time, irradiation resistance, and large-size production. This has enabled it to be broadly applied in high-energy physics experiments.[12] Over the past two decades, many GEM-based neutron detectors have been designed and constructed utilizing boron conversion material.[13–18] The CASCADE neutron detector was proposed and constructed at Heidelberg University,[13,16] and a spatial resolution of 2.6 mm was reached at ambient gas pressure. A neutron beam monitor using a GEM detector was developed at J-PARC[18] and it achieved good stability. In order to reduce the absorption and scattering effect by the GEM foil, a ceramic GEM has been developed for neutron detection at CSNS.[19] The experimental neutron transmittance results of the ceramic GEM demonstrated less absorption and scattering of thermal neutrons compared to the FR4 GEM. Many neutron detectors based on the ceramic GEM have been developed and put into engineering service at CSNS.[20–24]

In this paper, a large-area ceramic GEM detector prototype with an active area of about 307 mm×307 mm was developed. The neutron irradiation experiments for this detector, including beam profile imaging, spatial resolution, neutron wavelength spectrum determination, and measurement of the detection efficiency, were carried out at CSNS. The results demonstrate that the detector performs well and is suitable for beam-close neutron experiments.

2. Large-area ceramic GEM neutron detector

2.1. Principle and structure of the detector

To facilitate future upgrades of the detector to achieve high detection efficiency for thermal neutrons, the applied structure of the large-area ceramic GEM detector prototype is shown in Fig. 1. The detector is primarily composed of a 2D signal readout PCB and two GEM foils in combination with two boron-coated cathodes. It is a perfectly symmetric configuration with respect to the readout PCB in the middle of the detector's gas chamber. The cathode is a 100 μm thick aluminum (Al) film coated with a 1.0 μm thick B_4C converter layer where the abundance of ^{10}B is enriched to about 96%. When a neutron is captured by the ^{10}B atom, it undergoes a nuclear reaction n (^{10}B,^{7}Li) α that produces two energetic charged particles (α and ^{7}Li). They emit in opposite directions, and one of them escapes from the cathode and enters the working gas in the drift gap. This process leads to gas ionization, resulting in a significant number of electron–ion clusters, which represent the primary signal of the detector. Then the electrons among these charged clusters drift towards the GEM foil under the influence of an electric field and are multiplied in the GEM holes through the avalanche effect. This amplifies the detector's signal created by the neutron, achieving an improvement of the signal-to-noise ratio. Finally, induction signals are generated in the anode strips on the readout PCB as a result of the directional drift movement of multiplied electrons in the induction gap. It acts as the output signal of the boron-coated GEM neutron detector. In such a detector, the ions released from the cathode will form a long ionization track in the working gas, meaning that a neutron event can make one or more anode strips fire. To extract the 2D position information of incoming neutrons, a double-sided readout PCB with 512 cross-strips was designed and used in this detector. The pitch of the strips on the readout PCB is 1.2 mm and each strip is used as a readout channel for collecting the detector signal. The two symmetrical channels on the PCB surfaces are electrically connected, and half of the signal readout channels are assigned to the x direction and the others to the y direction. This forms a signal readout plane whose active area is equal to that of the GEM detector.

For experiments requiring the measurement of scattering neutrons with small angles with respect to the incident beam, the sensitive area of the neutron detector is expected to be large enough to cover the scattering angle range. In this paper, the sensitive area of this GEM foil is approximately 307 mm×307 mm, which is fabricated economically

by printed circuit board technology.[19] Its thickness is about 0.2 mm, the GEM holes (with 200 μm diameter) are arranged with 600 μm pitch, and a rim of 80 μm is etched for each GEM hole. To reduce the energy and propagation probability of discharges,[25] both surfaces of the GEM foil are segmented into six strips with a gap of about 2 mm (as illustrated in Fig. 2(a)), each of which is separately connected to the voltage supply through a high-value resistor of about 50 MΩ. In order to power the GEM detector, the high-voltage supply employs a parallel connection mode in which the single channel input delivers the voltage to whole sections on one side of the GEM foil. The GEM detector prototype is shown in Fig. 2(b). Its main body is made of Al alloy with a thin entrance window of 0.5 mm thickness. The gas chamber of the detector houses the cathodes, the GEM foils and the readout PCB. It is encapsulated with the HV circuit and the readout electronics system to constitute a compact GEM neutron detector, which reduces the impact of external electromagnetic interference on detector performance.

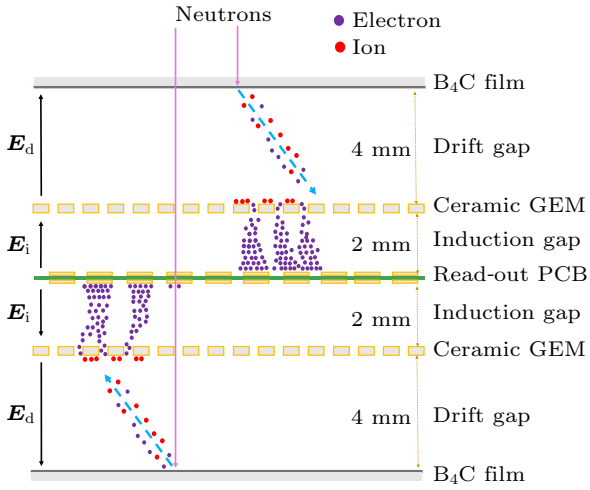


Fig. 1. The schematic drawing of the large-area GEM detector.

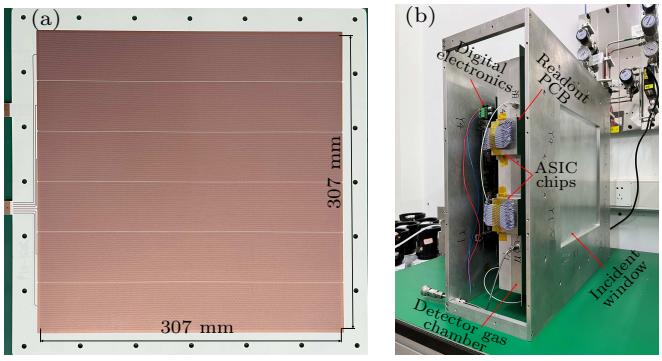


Fig. 2. (a) Photograph of the GEM foil and (b) photograph of the large-area ceramic-GEM detector prototype.

2.2. Readout electronics and DAQ system

The conventional and common ways to locate the position of incoming particles mainly include the charge centroid method and the time projection chamber method.[26] They can reconstruct the location of particle events with high accuracy, but have a shortcoming of slow speed at the event readout exits. This is mainly caused by the charge measurement of each detector channel fired in a neutron event. This suggests that the above two methods are not adapted to operational conditions under a high counting rate. In this work, we adopted the position coincidence method, in which the incident location of a neutron was recorded as the central point of those fired channels in an active event. It was combined with a fast signal provided by the GEM detector to achieve high-speed event reconstruction and data readout. To this end, a very fast readout electronics system has been constructed using eight analogue front-end readout chips and digital electronics based on modern field-programmable-gate-array (FPGA) technology. The detector's signals were read out using CIPix application-specified integrated circuit (ASIC) chips developed by the Heidelberg ASIC laboratory,[27] each of which integrated 64 channels of a low-noise charge-sensitive preamplifier followed by a shaper and a comparator. Then, the output signals were digitized at a clock rate of 10 MHz and fed into the digital electronics for performing the neutron event reconstruction. In addition, the CSNS's accelerator system provided the neutron instruments with 25 Hz synchronization signals and the pulse ID (pid), which give the time information of each neutron pulse. The former acted as the starting time, so-called t_0, for the neutron traveling in the TOF measurement, the latter was used to mark every t_0 signal. In order to obtain information about incident neutrons, there was a real-time event reconstruction algorithm configured in the FPGA to process the signals output from the ASIC chips. It was realized by a coincidence of correlation of fired channels in the time and space domain. Typically, the ionization event created by a neutron will fire one or more neighboring strips on the readout PCB and one or more continuous time bins (less than 400 ns), then, the central coordinates (x, y) of these neighboring strips were regarded as the hit position and the arrival time was recorded as t_1. This forms an active neutron event (x, y, t_1) detected by the detector. Furthermore, those neutron events registered in one proton pulse period were packaged into a data package in combination with the package head composed of the t_0, the pid and the total neutron counts in this pulse. The DAQ was connected to the readout electronics by a high-speed fiber to configure the parameters of the readout electronics and to collect the neutron data in real-time.

3. Simulation for the detector

Monte Carlo (MC) simulations were performed with FLUKA to evaluate the performance of this GEM detector prototype. To approximately treat and simplify the physical processes taking place in the detector, the calculation model used a simple configuration of the neutron source in combination with the detector whose inner structure is the same as a

real one. The electron multiplication stemming from the GEM foil and the detector signal collection process occurring in the induction region were not taken into account, and only the neutron reactions occurring in the converter and the energy deposition process in the drift region were involved. Moreover, it was reasonable and advisable to neglect the electron transverse diffusion in the working gas of the detector owing to the diffusion length being far less than the anode strip width on the readout PCB. To approach the conditions in a real position sensitive detector, a gas mixture Ar/CO_2 90:10 (by volume) with a gas pressure of 1 atm was set as the working gas in this detector model. The drift region with a 307 mm×307 mm active area was partitioned into a two-dimensional array, whose edge length was identical to the strip width on the readout PCB. The reconstructed position of a neutron event was regarded as the central point of those successive fired strips. Given the noise existing in the actual measurement condition, a reasonable energy threshold of 20 keV was applied in the simulations to determine whether the strip was fired or not, meaning that only the strip with deposited energy of over 20 keV could be treated as a valid one in a neutron event.

To verify the position resolution ability of this GEM detector, an ideal line source of thermal neutrons with 40 mm length was utilized in the simulations and the neutron beam was vertically incident to the detector. Figure 3 shows the reconstructed source images by the detector model and their position distributions. It can be seen in Figs. 3(a) and 3(c) that the 2D distribution reconstructed by the calculation model was a narrow strip of about 40 mm in length. This was in good agreement with the source size set in the simulation. The 2D distributions were respectively projected onto the x-axis and the y-axis, as shown in Figs. 3(b) and 3(d), and a Gaussian function was used to fit each projection to extract the spatial resolutions. The spatial resolution could be obtained from the formula FWHM $= 2.355 \times$ Sigma, where Sigma was the parameter of the fitting function and shown in the legend of the 1-D distribution. Thus, a simulated spatial resolution lower than 2.6 mm was attainable by the ceramic GEM detector.

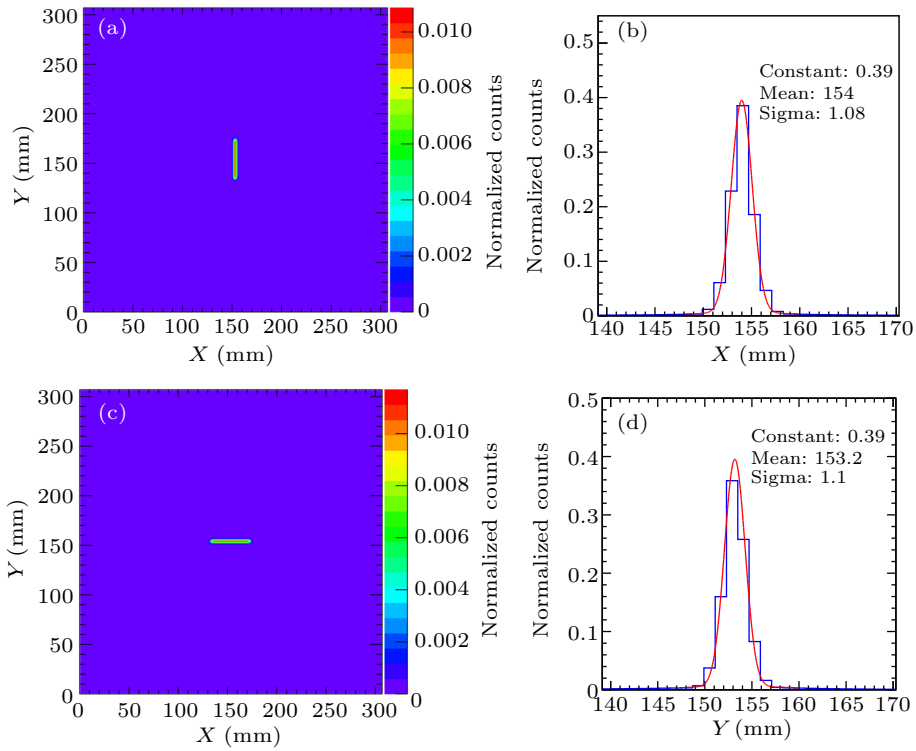


Fig. 3. Simulations of the spatial resolutions for the ceramic GEM detector.

4. Experiments and results

To evaluate the performance of the large-area ceramic GEM detector prototype, neutron irradiation experiments were carried out at the 20th beamline (BL20) of CSNS. The experimental measurements mainly included the plateau curve, the spatial resolution, the wavelength spectrum, the two-dimensional imaging capacity, and the detection efficiency. The neutron beam of the BL20 was drawn from the surface of the decoupled poisoned liquid hydrogen moderator and was collimated by the neutron guide and chopper system. The chopper system determined the wavelength range of the neutron beam from 1.0 Å to 5.5 Å, and the distance between the beam exit and the moderator surface was about 11.4 m. Additionally, in order to validate the range of the neutron wavelength resolved by this GEM detector prototype, a commercial neutron beam monitor with a detection efficiency of approximately 10^{-3}, ORDELA 4562N,[28] was used here for comparison.

4.1. Counting rate plateau

A proportional gaseous detector requires the working HV applied to the detector to be kept within the counting rate plateau, which illustrates that the plateau curve greatly influences normal detector operation. To obtain a proper working voltage of this GEM-based detector, the test of the counting rates was conducted with different high voltages from −1400 V to −2000 V at increments of 50 V, and the detector was placed 5.4 m away from the beam exit. The result is displayed in Fig. 4. The neutron events began to be recorded by the detector at the HV of −1500 V and the counting rate reached the plateau region at the HV of −1800 V. It is shown that the plateau slope of the detector was 2.3%/100 V with the plateau region covering −1800 V to −2000 V. For the sake of safety and stability of the detector operation, a working voltage of −1900 V was adopted to power the detector in subsequent measurements.

4.2. The 2D imaging and spatial resolution

Capabilities in terms of 2D imaging and spatial resolution were significant features of the large-area GEM detector. To lower the divergence of the neutron beam coming into the detector, a collimator with an aperture of 20 mm diameter was installed in front of the incident window of the detector, which limited the beam size and basically guaranteed the vertical incidence of neutrons. The result of the beam profile is shown in Fig. 5. It can be seen that the 2D imaging agrees well with the actual dimensions of the collimator and a low ratio of about 10^{-5} of the background to signal was reached. This demonstrated the good 2D imaging capacity of this GEM detector.

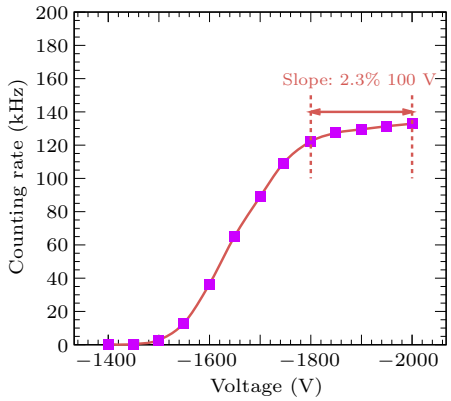


Fig. 4. Counting rate vs. working HV.

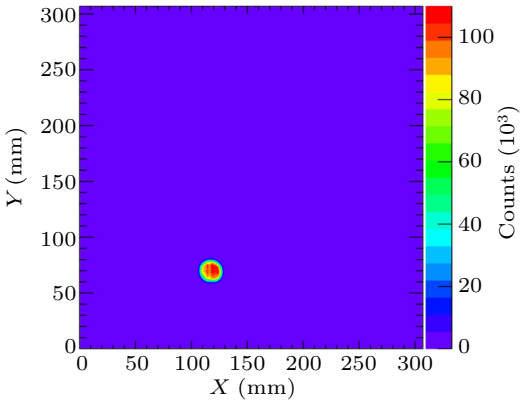


Fig. 5. Beam profile captured with a hole of 20 mm diameter.

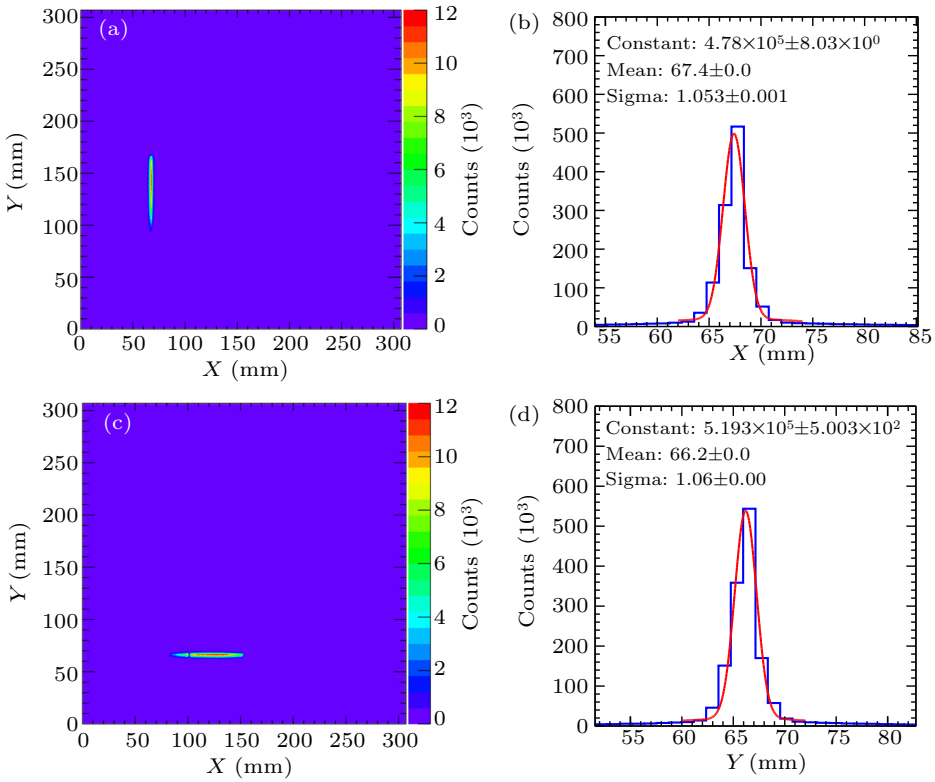


Fig. 6. Slit images and spatial resolutions: (a)–(b) *x*-direction and (c)–(d) *y*-direction.

The spatial resolution was measured with the linear-spread function method and we used a 2 mm-thick cadmium (Cd) mask with a slit of about 0.5 mm width to form a sufficiently narrow neutron beam in this work. The Cd mask was placed closely in front of the incident window of the detector, and the spatial resolutions of both directions were measured by rotating the Cd mask ninety degrees. Figure 6 shows the images of the slit and its 1D position distribution recorded by the detector. It is worth noting that the 2 imaging of the mask is straight and clear. The position resolution for the x-direction was below 2.48±0.01 mm (Fig. 6(b)), while the one for the y-direction was below 2.50±0.01 mm (Fig. 6(d)), where 0.01 mm is the statistical error. The experimental results agreed well with the simulated ones given by FLUKA (mentioned in Section 3) and manifested that the large-area GEM detector was able to measure the neutron beam in real-time with good spatial resolution. This basically satisfied the application requirements of the neutron instruments for mm-level spatial resolution, including SANS, VSANS and MR.

4.3. Wavelength spectrum

To verify the capacity of the resolved neutron wavelength of the GEM detector, the neutron wavelength spectrum was measured using the TOF method. In this test, a collimator with a hole of 5 mm diameter was set in front of the detector window to limit the neutron intensity of the incoming beam, which avoided the occurrence of detector saturation. A commercial neutron beam monitor was measured at the same site for comparison. Both of the spectra (from 0 Å to 6 Å) were corrected by their detection efficiencies calculated by FLUKA and normalized to the overall sum of counts. As displayed in Fig. 7, the neutron wavelength distribution captured by this detector was basically compatible with the one by the ORDELA 4562N monitor, and it was worth noting that there were obvious valley points at 4.05 Å and 4.68 Å. The two positions represented the Bragg edges of Al, which primarily originated from the neutron interaction with the aluminum components of the moderator shell and the detector window.

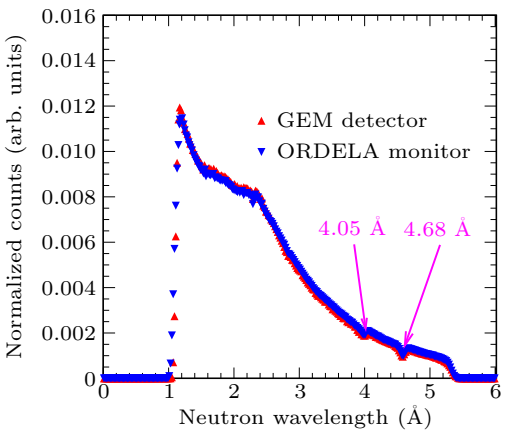


Fig. 7. Wavelength spectrum comparison of the GEM detector with the ORDELA 4562N beam monitor.

4.4. Detection efficiency

Detection efficiency is one of the crucial characteristics for large-area GEM neutron detector prototypes. Because of the continuous wavelength distribution of thermal neutrons delivered by the BL20, a neutron monochromator made of the mica crystal material, whose lattice spacing is 10.14 Å, was used in the experiment. It separates the neutrons with specific wavelengths from the incident beam and reduces the beam intensity coming from the detectors. The neutron detection efficiency of this detector was tested with a relative measurement and a 1 inch diameter standard counting tube filled with 20 atm ^{3}He gas was employed. The mica monochromator was placed in the path of the neutron beam and was deflected by forty-five degrees to select the monochromatic neutrons of 1.59 Å, 2.86 Å and 4.78 Å. To ensure the vertical incidence of the deflected beam along the diameter of the ^{3}He tube, we set a 2-mm-thick Cd plate with a hole of 0.5 mm diameter in front of the detectors. Moreover, the beam monitor (ORDELA 4562N) was mounted at the site of the beam exit to record the intensity of incident neutrons during the experiments. It was used to normalize the neutron counts respectively detected by the GEM detector and the ^{3}He tube. Then the detection efficiency of the large-area GEM neutron detector could be calculated by the following formula:

$$\eta_{\mathrm{Gem}} = \frac{N_{\mathrm{Gem}}}{N_{^3\mathrm{He}}} \cdot \eta_{^3\mathrm{He}}, \tag{1}$$

where $\eta_{^3\mathrm{He}}$ is the detection efficiency of the standard ^{3}He tube. It is 99.7% for 1.59 Å neutrons and nearly reaches 100.0% for 2.86 Å and 4.78 Å neutrons.

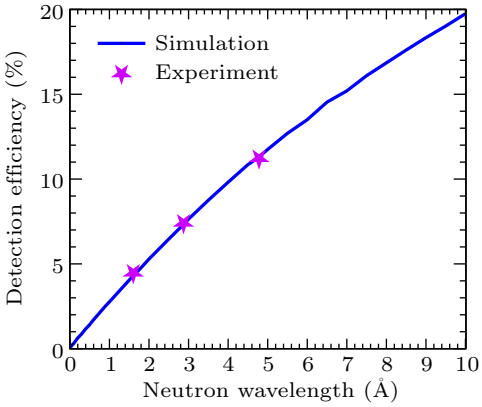


Fig. 8. The neutron detection efficiency given by the FLUKA simulation (blue curve) and the measurement (violet stars).

Thus, the measured detection efficiencies of the GEM detector prototype were respectively 4.7%±0.1% at 1.59 Å, 7.5%±0.1% at 2.86 Å and 11.2%±0.1% at 4.78 Å, where ±0.1% was the statistical error. To evaluate the efficiency values given by the experimental measurement, the detection efficiency curve of the GEM detector for neutrons with different wavelengths was simulated by FLUKA, as shown in Fig. 8. The simulation utilized the approach in Section 3 to

determine the valid neutron counts. It can be obtained that the simulated efficiencies were 4.6% for 1.59 Å neutrons, 7.6% for 2.86 Å neutrons and 11.6% for 4.78 Å neutrons, respectively. This indicates that the measured values of the detection efficiency were basically consistent with their simulated ones. Moreover, the difference of the detection efficiency between the simulated and measured values reached 0.4% at 4.78 Å, which mainly resulted from the neutron absorption caused by the readout PCB in the middle of the detector gas chamber and from a serious absorption effect taking place at longer wavelength.

5. Conclusion and outlook

In this paper, the feasibility of a large-area GEM detector prototype designed for neutron measurements under or close to the direct beam was verified. This GEM detector with an active area of about 307 mm×307 mm employed a symmetric structure with respect to the readout PCB. This configuration enhances the detection efficiency of the GEM detector and facilitates subsequent upgrades for higher efficiency. Capabilities in terms of the 2D imaging and the wavelength resolution were demonstrated, and the GEM detector exhibited good performance of the counting rate plateau with a slope of 2.3%/100 V ranging from −1800 V to −2000 V. The spatial resolution was tested experimentally to about 2.50±0.01 mm (FWHM), which agreed well with that simulated by FLUKA and satisfied the measurement demands of scattering neutrons and the beam profile. In addition, this detector prototype achieved a detection efficiency of 4.7% for neutrons with a wavelength of 1.59 Å, being in good agreement with the simulated value about 4.6%. In the future, a thinner readout PCB will be designed and fabricated to further reduce the neutron absorption effect; in addition, a large-area GEM detector with higher efficiency will be developed using a cascade of multiple layers of boron-coated GEM and will be equipped to the new neutron scattering instruments at CSNS.

Acknowledgements

Project supported by the National Key R&D Program of China (Grant No. 2023YFC2206502), the National Natural Science Foundation of China (Grant Nos. 12175254 and 12227810), Guangdong Major Project of Basic and Applied Basic Research (Grant No. 2023B0303000003), and Guangdong Provincial Key Laboratory of Advanced Particle Detection Technology (Grant No. 2024B1212010005).

References

[1] Mason T E, Abernathy D, Anderson I, *et al.* 2006 *Physica B* **385** 955
[2] Thomason J W 2019 *Nucl. Instrum. Methods Phys. Res. A* **917** 61
[3] Oyama Y 2006 *Nucl. Instrum. Methods Phys. Res. A* **562** 548
[4] Chen H S and Wang X L 2016 *Nat. Mater.* **15** 689
[5] Lindroos M, Bousson S, Calaga R, Danared H, Devanz G, Duperrier R, Eguia J, Eshraqi M, Gammino S, Hahn H, Jansson A, Oyon C, Pape-Møller S, Peggs S, Ponton A, Rathsman K, Ruber R, Satogata T and Trahern G 2011 *Nucl. Instrum. Methods Phys. Res. B* **269** 3258
[6] Ke Y B, He C Y, Zheng H B, Geng Y S, Fu J Y, Zhang S K, Hu H T, Wang S L, Zhou B, Wang F W and Tao J Z 2018 *Neutron News* **29** 14
[7] Zhu T, Zhan X Z, Xiao S W, Sun Y, Wu Y Y, Zhou A Y and Han Q F 2018 *Neutron News* **29** 11
[8] Chen J, Kang L and Lu H L 2018 *Physica B* **551** 370
[9] Xu J P, Xia Y G, Li Z D, Chen H C, Wang X L, Sun Z Z and Yin W 2021 *Nucl. Instrum. Methods Phys. Res. A* **1013** 165642
[10] Hendricks R W 1969 *Rev. Sci. Instrum.* **40** 1216
[11] Dana A S and Daniel M 2011 *The Helium-3 Shortage: Supply, Demand, and Options for Congress*
[12] Sauli F 2002 *Nucl. Instrum. Methods Phys. Res. A* **477** 1
[13] Klein M and Schmidt C J 2011 *Nucl. Instrum. Methods Phys. Res. A* **628** 9
[14] Uno S, Uchida T, Sekimoto M, Murakami T, Miyama K, Shoji M, Nakano E, Koike T, Morita K, Satoh H, Kamiyama T and Kiyanagi Y 2012 *Phys. Procedia* **26** 142
[15] Croci G, Cazzaniga C, Claps G, Tardocchi M, Rebai M, Murtas F, Vassallo E, Caniello R, Cippo E P, Grosso G, Rigato V and Gorini G 2014 *Prog. Theor. Exp. Phys.* **2014** 83
[16] Köhli M, Allmendinger F, Häußler W, Schröder T, Klein M, Meven M and Schmidt U 2016 *Nucl. Instrum. Methods Phys. Res. A* **828** 242
[17] Muraro A, Claps G, Croci G, Lai C C, Oliveira R D, Altieri S, Cancelli S, Gorini G, Hall-Wilton R, Höglund C, Cippo E P, Robinson L, Svensson P and Murtas F 2021 *Eur. Phys. J. Plus* **136** 742
[18] Ohshita H, Otomo T, Uno S, Ikeda K, Uchida T, Kaneko N, Koike T, Shoji M, Suzuya K, Seya T and Tsubota M 2012 *Nucl. Instrum. Methods Phys. Res. A* **672** 75
[19] Zhou J R, Zhou X J, Zhou J J, Jiang X F, Yang J Q, Zhu L, Yang W Q, Yang T, Xu H, Xia Y G, Yang G A, Xie Y G, Huang C Q and Hu B T, Sun Z J and Chen Y B 2020 *Nucl. Eng. Technol.* **52** 1277
[20] Zhou J R, Zhou X J, Zhou J J, Teng H Y, Yang J Q, Ma Y C, Zhou K, Xia Y G, Xiu Q L, Yang T, Jiang X F, Zhu L, Yang W Q, Yang G A, Xie Y G, Hu B T, Sun Z J and Chen Y B 2020 *Nucl. Instrum. Methods Phys. Res. Sect. A* **962** 163593
[21] Zhou J J, Zhou J R, Zhou X J, Zhu L, Wei Y D, Xu H, Guan B J, Wu H Y, Wei K, Yang J Q, Wu X G, Yang G A, Xie Y G, Zhang Y, Wang X H, Ding B W, Hu B T, Sun Z J, Duan L M and Chen Y B 2021 *Nucl. Instrum. Methods Phys. Res. A* **995** 165129
[22] Yang T, Zhou J R, Zhou X J, Zhu L, Zhu H Y, Zhou J J, Xia Y G, Wei Y D, Jiang X F, Yang W Q, Yang G A, Wang S L, Xie Y G, Sun Z J, Ouyang Q, Zhu J T and Chen Y B 2022 *IEEE Trans. Nucl. Sci.* **69** 68
[23] Zhu L, Zhou J R, Zeng L X, *et al.* 2023 *J. Instrum.* **18** P01033
[24] Tan J H, Zhou J R, Zhu L, et al. 2023 *Rev. Sci. Instrum.* **94** 103304
[25] Sauli F 2002 *Nucl. Instrum. Methods Phys. Res. A* **479** 294
[26] Kaminski J, Ball M, Bieser F, Janssen M, Kappler S, Ledermann B, Müller T, Ronan M and Wienemann P 2004 *Nucl. Instrum. Methods Phys. Res. A* **535** 201
[27] Becker J, Bösiger K, Lindfeld L, Müller K, Robmann P, Schmitt S, Schmitz C, Steiner S, Straumann U, Szeker K, Truöl P, Urban M, Vollhardt A, Werner N, Baumeister D, Löchner S and Hildebrandt M 2008 *Nucl. Instrum. Methods Phys. Res. A* **586** 190
[28] Neutron Beam Monitors https://ordela.com/neutron-beam-monitors/